APOBEC3F Is a Mutational Driver of the Human Monkeypox Virus Identified in the 2022 Outbreak

Rodolphe Suspène, Kyle A Raymond, Laetitia Boutin, Sophie Guillier, Frédéric Lemoine, Olivier Ferraris, Jean-Nicolas Tournier, Frédéric Iseni, Etienne Simon-Lorière, Jean-Pierre Vartanian

The Journal of Infectious Diseases
MAJOR ARTICLE

APOBEC3F Is a Mutational Driver of the Human Monkeypox Virus Identified in the 2022 Outbreak

Rodolphe Suspène,[1] Kyle A. Raymond,[1,2] Laetitia Boutin,[3,4] Sophie Guillier,[3] Frédéric Lemoine,[5,6,©] Olivier Ferraris,[3,4] Jean-Nicolas Tournier,[3,7] Frédéric Iseni,[3] Etienne Simon-Lorière,[5] and Jean-Pierre Vartanian[1]

[1]Virus and Cellular Stress Unit, Department of Virology, Institut Pasteur, Université de Paris Cité, Paris, France; [2]Sorbonne Université, Complexité du Vivant, Paris, France; [3]Microbiology and Infectious Diseases Department, Institut de Recherche Biomédicale des Armées, Brétigny-sur-Orge, France; [4]Institut de Recherche Biomédicale des Armées, National Reference Center for Orthopoxviruses, (CNR-LE Orthopoxvirus), Brétigny-sur-Orge, France; [5]Institut Pasteur, Université Paris Cité, G5 Evolutionary Genomics of RNA Viruses, Paris, France; [6]Institut Pasteur, Université Paris Cité, Bioinformatics and Biostatistics Hub, Paris, France; and [7]Ecole du Val-de-Grâce, Paris, France

Background. On May 6, 2022, a powerful outbreak of monkeypox virus (MPXV) had been reported outside of Africa, with many continuing new cases being reported around the world. Analysis of mutations among the 2 different lineages present in the 2021 and 2022 outbreaks revealed the presence of G->A mutations occurring in the 5′GpA context, indicative of APOBEC3 cytidine deaminase activity.

Methods. By using a sensitive polymerase chain reaction (differential DNA denaturation PCR) method allowing differential amplification of AT-rich DNA, we analyzed the level of APOBEC3-induced MPXV editing in infected cells and in patients.

Results. We demonstrate that G->A hypermutated MPXV genomes can be recovered experimentally from APOBEC3 transfection followed by MPXV infection. Here, among the 7 human APOBEC3 cytidine deaminases (A3A-A3C, A3DE, A3F–A3H), only APOBEC3F was capable of extensively deaminating cytidine residues in MPXV genomes. Hyperedited genomes were also recovered in ∼42% of analyzed patients. Moreover, we demonstrate that substantial repair of these mutations occurs. Upon selection, corrected G->A mutations escaping drift loss contribute to the MPXV evolution observed in the current epidemic.

Conclusions. Stochastic or transient overexpression of the *APOBEC3F* gene exposes the MPXV genome to a broad spectrum of mutations that may be modeling the mutational landscape after multiple cycles of viral replication.

Keywords. APOBEC3F; cytidine deaminase; monkeypox virus; outbreak; phylogeny.

Monkeypox (Mpox) is a neglected, zoonotic infectious disease caused by the Mpox virus (MPXV). This virus belonging to the *Orthopoxvirus* genus consists of a double-stranded, 197-kb deoxyribonucleic acid (DNA) genome. Monkeypox virus was first isolated in 1958 from a *Macaca fascicularis*, having originated from Singapore and imported to Copenhagen, which subsequently caused an outbreak in captive *Cynomolgus* monkeys [1]. By 1970, the virus proved capable of a zoonotic jump to humans, but it remained contained in Africa, causing isolated episodes of infection. This was until 2003, when an outbreak related to the import of small African mammals appeared in the United States [2]. In 2017, the largest Mpox outbreak in West Africa occurred in Nigeria [3], after decades of no identified cases. From 2018 to 2021, several cases had been imported from Nigeria to nonendemic countries such as United Kingdom, Israel, and Singapore [4–7]. In May 2022, a rapidly growing multicountry outbreak involving individuals without travel history to Mpox-endemic countries was identified. By July 23, 2022, the World Health Organization declared a Public Health Emergency of International Concern. As of April 13, 2023, 86 956 Mpox confirmed cases have been reported [8]. International sequencing efforts revealed that the 2022 outbreak virus belongs to MPXV clade IIb (part of the formerly designated "West African" clade) [9] and forms a divergent lineage (B.1) that descends from genomes related to the 2017–2018 outbreak in Nigeria [10].

The extent of the divergence of the 2022 outbreak genomes from the related 2018–2019 viruses is striking, considering the estimated substitution rate for orthopoxviruses [11]. The most accumulated mutations in the 2022 MPXV genomes (42 of 47 mutations) correspond to cytidine (C) to thymine (T) (C->T) transitions, occurring in the 5′TpC context (5′TpC->TpT or 5′GpA->ApA in the reverse strand) [12, 13]. This mutation signature is unique but pervasive in recent clade IIb genomes, with significant signal in sublineage branches. More importantly, this signature is absent from clade I, IIa or older clade IIb MPXV genomes and brings to the forefront the recent activity of APOBEC3 (A3) cytidine deaminases [10, 14, 15].

In the last 2 decades, it has emerged that the human A3 locus encodes 6 functional polynucleotide cytidine deaminases (A3A, A3B, A3C, A3F, A3G, and A3H) [16], originally described as

Received 14 February 2023; editorial decision 14 February 2023; accepted 12 May 2023; published online 24 May 2023

Correspondence: Jean-Pierre Vartanian, PhD, Department of Virology, Institut Pasteur, 28 rue du Dr. Roux, 75724 cedex 15 Paris, France (jean-pierre.vartanian@pasteur.fr).

The Journal of Infectious Diseases® 2023;228:1421–9

https://doi.org/10.1093/infdis/jiad165

innate cellular restriction factors against viruses and retroelements through the deamination of C to U in single-stranded DNA [17–22]. These deamination events occur preferentially in the context of 5′TpC, with the exception of A3G, which prefers 5′CpC dinucleotides [23–26].

In this work, we demonstrated that G->A hypermutated MPXV genomes can be recovered experimentally from A3F transfection followed by MPXV infection. In addition, hyperedited MPXV genomes were recovered in ∼42% of analyzed patients, indicating that editing occurs in vivo.

METHODS

Cells and Virus

HeLa cells (human epithelial cells; CCL-2, ATCC) were maintained in Dulbecco's modified Eagle's medium (DMEM, Gibco), supplemented with heat-inactivated fetal calf serum (10%), penicillin (50 U/mL), and streptomycin (50 mg/mL) and were grown in 75-cm^2 cell culture flasks in a humidified atmosphere containing 5% CO_2.

A virus from the 2022 MPXV outbreak was isolated, and a stock was produced on Vero cells [27]. Passage 2 stock was titered by plaque-forming assay in 24-well plates and sequenced. The obtained titer was 2×10^6 plaque-forming units/mL.

Transfection, Viral Infections, Differential DNA Denaturation Polymerase Chain Reaction, Cloning and Sequencing

Transfections were performed independently in triplicate on HeLa cells. Briefly, 2.5×10^5 HeLa cells were transfected with 1 μg of individual plasmids encoding either A3A, A3B, A3C, A3F, A3G, A3H, or an empty plasmid (ep) as control, using jetPRIME (Polyplus). At 24 hours posttransfection, HeLa cells were infected with MPXV at a multiplicity of infection of 1 for 24 hours. Total DNA from HeLa-infected cells was extracted with the QiAmp DNA Mini kit (QIAGEN). Differential DNA denaturation polymerase chain reaction (3D-PCR) was performed on an Eppendorf gradient Master S programmed to generate a 78°C–82°C or 76°C–86°C gradient in the denaturation temperature (Td). This technique relies on the fact that AT-rich DNA denatures at a lower temperature than GC-rich DNA [28] and has proven successful at selectively amplifying APOBEC3-edited viral DNA for hepatitis B virus [29, 30], papillomaviruses (human papillomavirus) [31], herpesviruses (herpes simplex virus, Epstein-Barr virus) [32] as well as for viruses with a DNA intermediate, such as retroviruses [33, 34].

A fragment of the *B10R ER-localized apoptosis regulator* (*Cop-B9R*) gene position (nucleotide 168241–168906, GenBank accession MT903344) was amplified by using a nested procedure. For the in vitro experiments, the first-round primers were 5′ GACTAAATTTCTCGGTAGCACATCGAA and 5′ GGGACACCTGTATTCATGTTACTGAA. First PCR conditions were as follows: 5 minutes 95°C then (1 minute 95°C, 1 minute 58°C, 2 minutes 72°C) × 42 cycles. The PCR products were purified from agarose gels (NucleoSpin Gel and PCR Clean-up; Macherey-Nagel). Nested PCR (position, 168303–168445) was performed with 1/100 of the purified first-round PCR products, primers were 5′ CTATCATCTACTCAA TGTCTATTAGACG and 5′GTTCTGTACATTGATCATA TATAACTACTC, and amplification conditions were as follows: 5 minutes 95°C then (30 seconds 78°C–82°C, 30 seconds 58°C, 1 minute 72°C) × 45 cycles, then 20 minutes 72°C.

For the PCR amplification of MPXV from patients, the first-round primers were identical to the in vitro amplification. Nested PCR (nucleotide 168240 to 168487) was performed with 1/100 of the purified first-round PCR products, primers were 5′ TAACGCCCTTGGCTCTAACCATTTTCAA and 5′ GACGTGTTTGTTGAGTATCGGTGATAA, and amplification conditions were as follows: 5 minutes 95°C then (30 seconds 76°C–86°C, 30 seconds 58°C, 1 minute 72°C) × 45 cycles, then 20 minutes 72°C. The choice to use different internal primers during the 3D-PCR for the experiments performed in vitro provided a higher heterogeneity of MPXV populations, thus facilitating the mutational analysis.

The 3D-PCR products were purified from agarose gels (NucleoSpin Gel and PCR Clean-up) and ligated into the TOPO TA cloning vector (Invitrogen), and ∼20–100 colonies were sequenced. A minimum threshold of 2 G->A transitions per sequence was imposed to reduce the impact of MPXV natural variation and PCR error in designating A3 editing.

Phylogenetic Analyses

We retrieved all complete or near-complete MPXV sequences available on GenBank as of July 4, 2022. Sequences were aligned to reference sequence (accession MT903344) using MAFFT v7.467 (option –thread 20 –auto –keeplength –addfragments), and positions 0–1500, 2300–3600, 6400–7500, 133050–133250, 173250–173460, and 196233-end were masked (replaced with N) using goalign v0.35 [35] (options mask –s<start > -l). The latter step avoids keeping sites that contain interfering phylogenetic signal (regions with too much diversity, with long homopolymers or repetitive elements). From this multiple sequence alignment, a phylogenetic tree with bootstrap supports was inferred using IQ-TREE 2 v2.0.6 (options -nt 20 –safe -m GTR + G4 + FO –seed 123456789 -b 100) [36]. The tree was rooted using the sequence NC_003310 as outgroup (concordant with the root detected by temporal signal using Tempest v1.5.3 [37]). Ancestral sequences at each internal node of the phylogeny were inferred using raxml-ng v1.0.1 [38] (options –ancestral –msa <msa > –tree < iqtree tree > –model GTR + G4 + FO), and all mutations corresponding to branches of interest were counted using a dedicated script.

To compute the expected number of each type of mutation, we simulated sequences along the tree (at internal nodes and tips), 100 times, using seq-gen v1.3.4 (https://github.com/

rambaut/Seq-Gen), taking the inferred ancestral sequence as the root sequence, with GTR model and the parameter values (rate parameters, state frequencies, and alpha parameter of the gamma distribution) initially optimized by IQ-TREE 2 while inferring the tree. We then counted the mutations between internal node sequences corresponding to branches of interest and averaged the number of mutations over the 100 simulations.

Sanger Sequencing Data Analysis

We preprocessed the isolate sequence (GenBank accession no. ON755039), to keep the subsequence from positions 168239 to 168487 (numbering according to the reference sequence, GenBank accession no. MT903344), using goalign v0.3.6a (options subseq –s<start > -l). We then mapped the sequences of all the samples to this reference using minimap v2.24 [39] (options -a -x splice –sam-hit-only –secondary = no –score-N = 0). We converted the sam files to a multiple sequence alignment using gofasta v1.1.0 [40] (options sam toMultiAlign -s<sam > –start 168240 –end 168487). We then removed sequences having more than 70% N using goalign v0.3.6a (options clean seqs –char N -c 0.7). Alignment and Sanger sequence traces were visually inspected using Geneious Prime (Biomatters Ltd.) We finally counted the different mutations and their context on the reference sequence using a python script (https://github.com/Simon-LoriereLab/MPXV_apo).

Ethical Statement

The IRBA is the national reference center for orthopoxviruses (Le Centre National de Référence Laboratoire Expert Orthopoxvirus), designated by the French Ministry of Health (through the "*Arrêté du 7 mars 2017 fixant la liste des centres nationaux de référence pour la lutte contre les maladies transmissibles*") to process the samples for identification and characterization of MPXV. The patient signed an informed consent, and the sample subjected to viral genetic characterization was processed in an anonymized fashion. All work with infectious virus was performed in biosafety level 3 containment laboratories.

RESULTS

To visualize the presence of the A3 signature, a phylogenetic tree representing the clade I, IIa, and IIb genomes was generated (Figure 1). The tree presents the number and nucleotide context of each type of mutations (colored bars) that occurred at different branches (between inferred ancestral sequences). This shows a clear signature starting from clade A.2 and A.1 that is not expected under the substitution model used for tree inference (empty bars). In particular, we observed a significantly high overrepresentation of 5′TpC->TpT mutations (5′GpA->ApA in the reverse strand), suggesting that the analyzed context is not indicative with A3G-induced editing [41], and a high underrepresentation of the other mutations in these clades, compared to the base model and to the other clades. A complete phylogeny with tip names is presented in Supplementary Figure 1. These monotonous mutations, occurring in a specific context, reflects the footprint of an A3 cytidine deaminase and confirm the findings observed by previous studies [10, 12, 15, 41–43].

To determine whether A3 enzymes are capable of editing MPXV genomes, HeLa cells were transfected with A3A, A3B, A3C, A3F, A3G, A3H, or with an ep used as a negative control, and then infected with a low passage 2022 MPXV isolate [27]. A3DE is a nonfunctional enzyme and was not used in this study [44]. The use of HeLa cells is not physiological; however, in vitro assays have shown that these cells are susceptible and capable of maintaining MPXV replication, resulting in a high titer virus stock [45, 46].

Differential DNA denaturation polymerase chain reaction (3D-PCR) was used to detect and selectively amplify AT-rich edited genomes located in MPXV *B10R ER-localized apoptosis regulator* (*Cop-B9R*) gene [28]. As shown in Figure 2A, 81.2°C was the minimal temperature that allowed amplification of the MPXV genome with A3A, A3B, A3C, A3G, A3H, and ep. Specifically, it was possible with A3F overexpression to selectively amplify MPXV DNA at 80.7°C, indicating a higher mutational burden. The A3F enzyme was able to extensively deaminate MPXV DNA (Figure 2B), with the complete sequences presented in Supplementary Figure 2. Sequencing revealed extensive and monotonous cytidine deamination of both DNA strands (Figure 2C). We determined that the mean of G->A editing frequency was ∼22% (range, 5%–79% per clone). Analysis of the dinucleotide context of edited sites showed a strong 5′ effect favoring 5′GpA (5′TpC in the opposite DNA strand) typical of A3F enzyme [23–26] (Figure 2D). By contrast, there was no pronounced 3′ nucleotide context, such as 5′CpG, thus ruling out a cytidine hypermethylation/deamination-related phenomenon (data not shown).

Next, we tested whether edited MPXV genomes could be detected in patients. The 3D-PCR was performed on DNA extracted from 24 MPXV-infected patients presented in Supplementary Table 1. A Td gradient from 77°C–82°C was performed with the latest Td presented (Figure 3A). The 3D-PCR products were recovered at a Td as low as (1) 78.6°C for patients 10, 15, and 20 and (2) 25°C and 79.9°C for patients 02, 04, 18, and 27. Comparatively, we observed that editing by A3F has a Td = 79°C. These Tds were below the limiting Td = 81.2°C corresponding to unedited DNA obtained with the ep transfection or with a molecular clone of MPXV. It is interesting to note that MPXV detected with a Td = 81.4°C for patients 03, 05, 07, 11, 12, 13, 14, 16, 19, 23, 24, 28, 29, and 30 are not edited either. Finally, when considering the most selective Td by 3D-PCR, we observed that 10 of the 24 (∼42%) patient

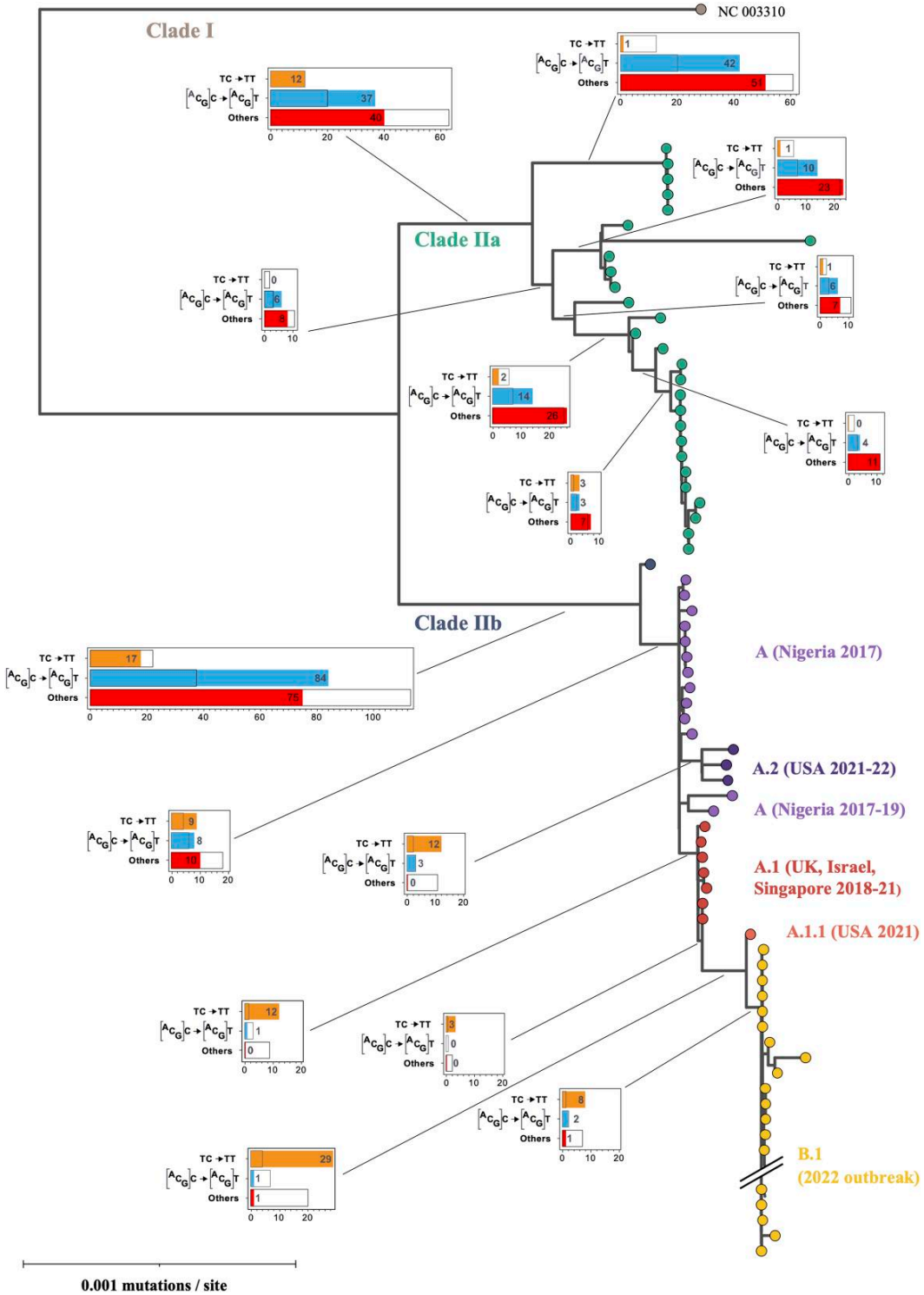

Figure 1. Phylogenetic analysis of substitutions within monkeypox virus clade IIa and IIb. A maximum likelihood tree was inferred using IQ-TREE2. The observed number of each type of mutations are indicated in the filled bar plots along each branch of the phylogeny. The orange and blue boxes indicate, respectively, the C->T mutations occurring in the 5′TpC->TpT and 5′(A or C or G)pC->(A or C or G)pT contexts, whereas the red boxes indicate all other types of mutations. Empty bar plots represent the average number of mutations obtained over 100 simulations under the substitution model used for tree inference. Tree scale is given in number of mutations per site, as output by phylogenetic inference software.

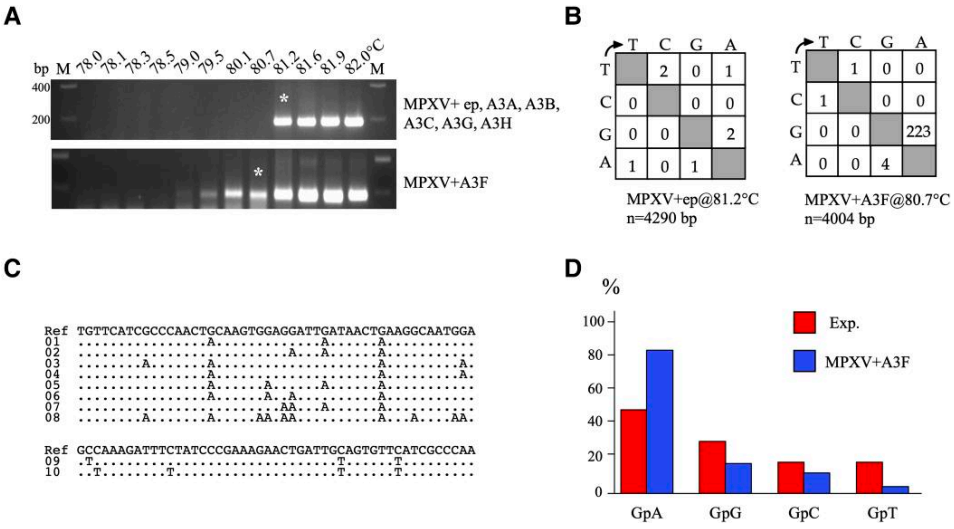

Figure 2. APOBEC3F editing of monkeypox virus (MPXV) DNA. (A) Differential DNA denaturation polymerase chain reaction (3D-PCR) recovered A3F and empty plasmid vector, A3A-A3C, A3G, A3H-edited MPXV genomes down to 80.7°C and 81.2°C, respectively. Asterisks refer to the samples cloned and sequenced. (B) Mutation matrices for hyperedited *Cop-B9R* sequences derived from cloned 80.7°C and 81.2°C 3D-PCR products. n indicates the number of bases sequenced and corresponds to 28 and 30 sequences × 143 base pairs (bp) for ep or A3F + MPXV, respectively. (C) A selection of hypermutated A3F G->A and C->T edited MPXV genomes (denaturation temperature = 80.7°C). Although editing may occur on both strands, the sequences are given with respect to the plus or coding strands. Only differences are shown. All sequences were unique, indicating that they corresponded to distinct molecular events. (D) Bulk dinucleotide context of MPXV *Cop-B9R* gene fragment by A3F cytidine deaminase and compared with the expected values. The red bars represent the expected frequencies assuming that G->A transitions were independent of the dinucleotide context and correspond to the weighted mean dinucleotide composition of the reference sequence (GenBank accession no. MT903344). The blue bars represent the percentage of G->A transitions occurring within 5′GpN dinucleotides for the hypermutated sequences. bp, base pair; ep, empty plasmid vector and MPXV alone; M, molecular weight markers.

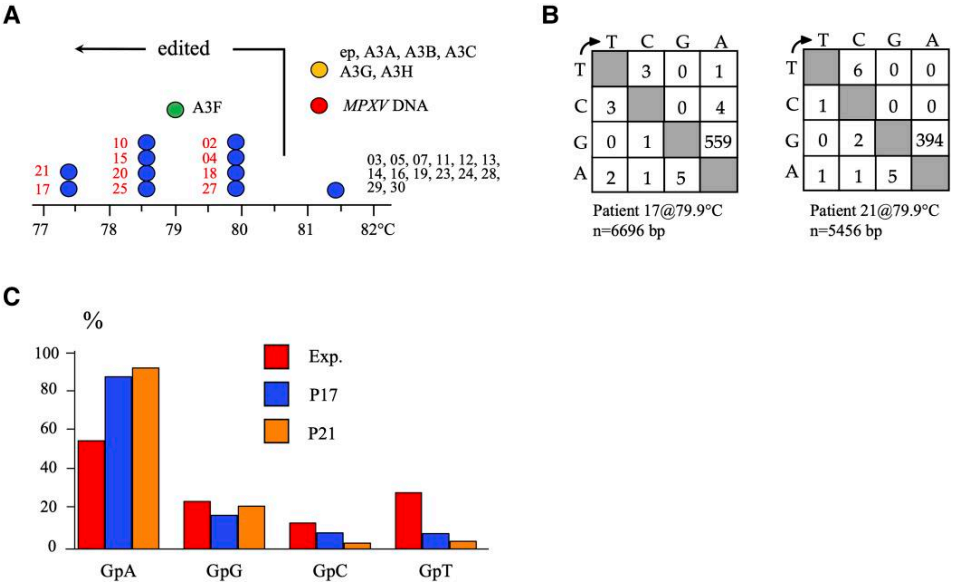

Figure 3. APOBEC3 editing of monkeypox virus (MPXV) in vivo. (A) Schematic representation of the denaturation temperature (Td) for the last positive differential DNA denaturation polymerase chain reaction amplifications for 24 patients infected with MPXV (dark blue circles). The arrow indicates the threshold Td (80.7°C) at which the samples are hypermutated. The samples in red were cloned and sequenced. The red, orange, and green circles represent, respectively, the last Td of the MPXV DNA molecular clone corresponding to the reference sequence, empty plasmid, A3A–A3C, A3G, A3H, and A3F. (B) Mutation matrices for hyperedited *Cop-B9R* sequences derived from patients 17 and 21 at 79.9°C, n indicates the number of bases sequenced and corresponds to 27 and 22 G->A sequences × 248 base pairs (bp) for patients 17 and 21, respectively. (C) Bulk dinucleotide context of MPXV *Cop-B9R* gene fragment for patients 17 and 21 and compared with the expected values.

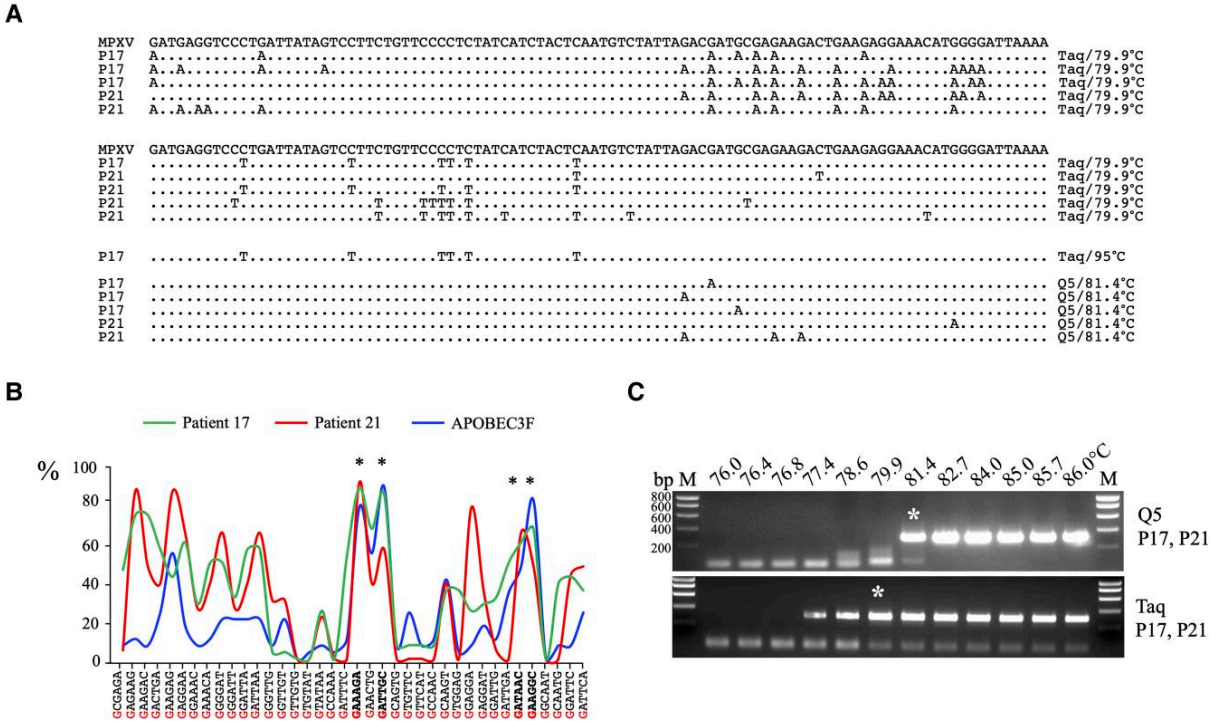

Figure 4. Hypermutation of monkeypox virus (MPXV) DNA in vitro and in vivo. (A) A selection of hypermutated MPXV sequences from patients 17 and 21 (denaturation temperature = 95°C, 81.4°C, and 79.9°C) is shown and compared with the reference. The sequence is given with respect to the viral plus strand. Only differences are shown. All sequences were unique, indicating that they corresponded to distinct molecular events. (B) Site-specific frequency analysis of editing from A3F-transfected cells and from patients 17 and 21 recovered by differential DNA denaturation polymerase chain reaction (3D-PCR). The stars represent the overlapping hot spot with the context in bold. Analysis was performed from nucleotide 168303–168445, accounting for 38 Gs. (C) The 3D-PCR amplification across a 76°C–86°C gradient using either Taq or Q5 DNA polymerase, the latter fails to amplify DNA containing dU, the product of A3 deamination. Asterisks indicate the PCR products cloned and sequenced. bp, base pair; M, molecular weight markers.

samples analyzed exhibited hypermutated sequences (Figure 3A, samples in red validated by sequencing).

In light of these data, we decided to analyze patients 17 and 21 in detail, because they presented the most hyperedited viruses, as visualized by the last Td obtained and the mutation matrices (Figure 3A and B). As observed in Figure 4A and Supplementary Figure 2, at Td = 79.9°C, G->A and C->T hyperedited genomes were found in patients 17 and 21, proving that both DNA strands could be edited (Taq/79.9°C). The mean editing frequency of G->A was similar between the 2 patients ~38% and ~32% (range, 14%–47% and 16%–58% for patient 17 and 21, respectively). By analyzing the editing frequencies obtained with a Td = 95°C, we were able to determine that the in vivo frequency of hypermutants is ~1.75% (1 hypermutant detected among 58 sequences, patient 17), proving that this phenomenon is not a rare event (Figure 4A, Supplementary Figure 2).

The dinucleotide context associated with G->A hyperedited genomes in vivo showed an overall preference for 5′GpA (5′ TpC in the opposite DNA strand) (Figure 3C), which is comparable to those detected in vitro (Figure 2D). By comparing the mutational frequency of MPXV DNA from patients 17 and 21 at each of the 38-target G residues with those derived from the A3F transfection, significant correlations with the presence of mutational hotspots were observed between the in vitro and in vivo edited sites (Figure 4B, Supplementary Figure 2). This collection of evidence clearly indicates that the main mutator enzyme of the MPXV genome in vivo is A3F; however, it is not excluded that other A3s could be involved in MPXV editing both in vitro and in vivo.

Upon A3-induced cytidine deamination, DNA bearing multiple dU residues may be corrected by the MPXV UNG (uracyl *N*-glycosylase) pathway, or, if copied on the opposite strand, the resulting dU:dA base pair might be proofread to dT:dA. The function of this enzyme is to prevent mutagenesis by cleaving uracil from DNA molecules by removing the *N*-glycosidic bond and triggering the base excision repair pathway. To explore this issue, we performed the first round PCR using either Q5 or Taq polymerases on extracted DNA from patients 17 and 21 lesions. Like all archaeal DNA polymerases, Q5 is unable to

amplify DNA templates bearing dU [47]: if only 1 of the many existing dUs is uncorrected, the genome will not be amplified by the Q5. To assess the efficacy of the MPXV UNG repair system, 3D-PCR products obtained at Td = 79.9°C and 81.4°C with Taq and Q5 polymerases, respectively, were cloned and sequenced (Figure 4C, Supplementary Figure 2). As can be observed, Q5 amplification recovered less edited DNA than Taq polymerase, indicating that some dU:dA pairs can be repaired to dT:dA. These observations indicate that substantial repair does occur, demonstrating that upon selection, corrected G->A mutations that escape drift loss are contributing to the MPXV evolution as observed in the current epidemics.

DISCUSSION

We have demonstrated that the MPXV viral mutations observed during the successive outbreaks of 2017–2019 and 2022 are in part the consequence of A3F cytidine deaminase activity. The library of hypermutated MPXV genomes identified presented a range of editing from ~5% to 79% (Supplementary Figure 2). These data show that there is a range of mutations among the analyzed sequences, demonstrating a balance between A3-associated hypo- and hyperediting of the MPXV genome. Hyperediting frequency detected can be phenomenally high, $>10^{-1}$ per base, so much so that they result in defective viruses. On the contrary, hypoediting rates are lower, perhaps at the order of 10^{-6} per base. Obviously, only limited deamination of viral genomes is likely to generate viruses presenting fitness compatible with further transmission and thus have the chance to be fixed in a successful viral lineage.

Several DNA viruses have been documented to exhibit mechanisms that limit or counteract the effects of A3 enzymes, such as coding for a viral interactor, preventing A3 incorporation into virions, replicating in cells with low or absent A3 expression, or replicating in preferred subcellular locations. The efficacy of these mechanisms may differ in MPXV lineage B viruses compared to other lineages, but it is also conceivable that ecological shifts, including sustained human-to-human transmission in sufficient numbers, may have led to the detectable occurrence of this process.

CONCLUSIONS

Further genomic surveillance will show whether fortuitous founder events contributed to the genetic make-up of the genomes detected in the 2022 outbreak, and whether this process will continue to play a role in the evolution of MPXV in the ongoing outbreak. Indeed, this protective mechanism may eventually contribute to evolutionary jumps or increased evolutionary rates, that could be associated with viral immune escape or resistance to treatment. Understanding the mechanisms involved behind this editing process could lead to promising new antiviral approaches against MPXV.

Supplementary Data

Supplementary materials are available at *The Journal of Infectious Diseases* online. Consisting of data provided by the authors to benefit the reader, the posted materials are not copyedited and are the sole responsibility of the authors, so questions or comments should be addressed to the corresponding author.

Notes

Acknowledgments. We thank all healthcare workers, public health employees, and scientists involved in the monkeypox outbreak response. We acknowledge the authors and contributing laboratories for submitting the monkeypox virus sequences to GenBank. This work used the computational and storage services provided by the IT department at Institut Pasteur, Paris.

Author contributions. RS and JPV designed research, RS, KAR, SG, and LB performed experiments; FL and ES-L performed phylogenetic analysis; RS, KAR, SG, LB, FL, OF, J-NT, FI, ES-L, and J-PV analyzed data; RS, KAR, ES-L, and J-PV wrote the paper with inputs from all authors.

Financial support. This work was supported by grants from the Institut Pasteur and Centre National de la Recherche Scientifique. KAR was supported by Allocation de Recherche du Ministère de la Recherche et de l'Enseignement Supérieur. OF, LB, and J-NT acknowledge the support from Santé Publique France for the Le Centre National de Référence Laboratoire Expert Orthopoxvirus. FI acknowledges funding from the Direction Générale de l'Armement (Biomedef PDH-2-NRBC-4-B-4111). ES-L acknowledges funding from the INCEPTION program (Investissements d'Avenir Grant ANR-16-CONV-0005), PICREID program (Award Number U01AI151758), and Labex IBEID (ANR-10-LABX-62-IBEID).

Potential conflicts of interest. All authors: No reported conflicts of interest.

References

1. Magnus PV, Andersen E, Petersen K, Birch-Andersen A. A pox-like disease in cynomolgus monkeys. Acta Pathol Microbiol Scand **1959**; 46:156–76.
2. Centers for Disease Control and Prevention (CDC), Multistate outbreak of monkeypox–Illinois, Indiana, and Wisconsin, 2003. MMWR Morb Mort Wkly Rep **2003**; 52:537–40.
3. Yinka-Ogunleye A, Aruna O, Dalhat M, et al. Outbreak of human monkeypox in Nigeria in 2017-18: a clinical and epidemiological report. Lancet Infect Dis **2019**; 19:872–9.
4. Erez N, Achdout H, Milrot E, et al. Diagnosis of imported monkeypox, Israel, 2018. Emerg Infect Dis **2019**; 25:980–3.
5. Mauldin MR, McCollum AM, Nakazawa YJ, et al. Exportation of monkeypox virus from the African continent. J Infect Dis **2022**; 225:1367–76.
6. Ng OT, Lee V, Marimuthu K, et al. A case of imported monkeypox in Singapore. Lancet Infect Dis **2019**; 19:1166.

7. Vaughan A, Aarons E, Astbury J, et al. Two cases of monkeypox imported to the United Kingdom, September 2018. Euro Surveill **2018**; 23:1800509.
8. Centers for Disease Control and Prevention. Available at: https://www.cdc.gov/poxvirus/mpox/response/2022/world-map.html
9. Happi C, Adetifa I, Mbala P, et al. Urgent need for a non-discriminatory and non-stigmatizing nomenclature for monkeypox virus. PLoS Biol **2022**; 20:e3001769.
10. Isidro J, Borges V, Pinto M, et al. Phylogenomic characterization and signs of microevolution in the 2022 multi-country outbreak of monkeypox virus. Nat Med **2022**; 28:1569–72.
11. Firth C, Kitchen A, Shapiro B, Suchard MA, Holmes EC, Rambaut A. Using time-structured data to estimate evolutionary rates of double-stranded DNA viruses. Mol Biol Evol **2010**; 27:2038–51.
12. Forni D, Cagliani R, Pozzoli U, Sironi M. An APOBEC3 mutational signature in the genomes of human-infecting orthopoxviruses. mSphere **2023**;8:e0006223.
13. O'Toole A, Neher RA, Ndodo N, et al. Putative APOBEC3 deaminase editing in MPXV as evidence for sustained human transmission since at least 2016. Available at: https://doiorg/101101/20230123525187. Accessed January 24, 2023.
14. Chen Y, Li M, Fan H. The monkeypox outbreak in 2022: adaptive evolution associated with APOBEC3 may account for. Signal Transduct Target Ther **2022**; 7:323.
15. Dobrovolna M, Brazda V, Warner EF, Bidula S. Inverted repeats in the monkeypox virus genome are hot spots for mutation. J Med Virol **2023**; 95:e28322.
16. Jarmuz A, Chester A, Bayliss J, et al. An anthropoid-specific locus of orphan C to U RNA-editing enzymes on chromosome 22. Genomics **2002**; 79:285–96.
17. Harris RS, Bishop KN, Sheehy AM, et al. DNA deamination mediates innate immunity to retroviral infection. Cell **2003**; 113:803–9.
18. Lecossier D, Bouchonnet F, Clavel F, Hance AJ. Hypermutation of HIV-1 DNA in the absence of the Vif protein. Science **2003**; 300:1112.
19. Mangeat B, Turelli P, Caron G, Friedli M, Perrin L, Trono D. Broad antiretroviral defence by human APOBEC3G through lethal editing of nascent reverse transcripts. Nature **2003**; 424:99–103.
20. Mariani R, Chen D, Schrofelbauer B, et al. Species-specific exclusion of APOBEC3G from HIV-1 virions by Vif. Cell **2003**; 114:21–31.
21. Sheehy AM, Gaddis NC, Choi JD, Malim MH. Isolation of a human gene that inhibits HIV-1 infection and is suppressed by the viral Vif protein. Nature **2002**; 418:646–50.
22. Zhang H, Yang B, Pomerantz RJ, Zhang C, Arunachalam SC, Gao L. The cytidine deaminase CEM15 induces hypermutation in newly synthesized HIV-1 DNA. Nature **2003**; 424:94–8.
23. Beale RC, Petersen-Mahrt SK, Watt IN, Harris RS, Rada C, Neuberger MS. Comparison of the differential context-dependence of DNA deamination by APOBEC enzymes: correlation with mutation spectra in vivo. J Mol Biol **2004**; 337:585–96.
24. Bishop KN, Holmes RK, Sheehy AM, Davidson NO, Cho SJ, Malim MH. Cytidine deamination of retroviral DNA by diverse APOBEC proteins. Curr Biol **2004**; 14:1392–6.
25. Liddament MT, Brown WL, Schumacher AJ, Harris RS. APOBEC3F properties and hypermutation preferences indicate activity against HIV-1 in vivo. Curr Biol **2004**; 14: 1385–91.
26. Suspène R, Sommer P, Henry M, et al. APOBEC3G Is a single-stranded DNA cytidine deaminase and functions independently of HIV reverse transcriptase. Nucleic Acids Res **2004**; 32:2421–9.
27. Frenois-Veyrat G, Gallardo F, Gorge O, et al. Tecovirimat is effective against human monkeypox virus in vitro at nanomolar concentrations. Nat Microbiol **2022**; 7:1951–5.
28. Suspène R, Henry M, Guillot S, Wain-Hobson S, Vartanian JP. Recovery of APOBEC3-edited human immunodeficiency virus G->A hypermutants by differential DNA denaturation PCR. J Gen Virol **2005**; 86:125–9.
29. Suspène R, Guétard D, Henry M, Sommer P, Wain-Hobson S, Vartanian JP. Extensive editing of both hepatitis B virus DNA strands by APOBEC3 cytidine deaminases in vitro and in vivo. Proc Natl Acad Sci USA **2005**; 102:8321–6.
30. Turelli P, Mangeat B, Jost S, Vianin S, Trono D. Inhibition of hepatitis B virus replication by APOBEC3G. Science **2004**; 303:1829.
31. Vartanian JP, Guétard D, Henry M, Wain-Hobson S. Evidence for editing of human papillomavirus DNA by APOBEC3 in benign and precancerous lesions. Science **2008**; 320:230–3.
32. Suspène R, Aynaud MM, Koch S, et al. Genetic editing of herpes simplex virus 1 and epstein-barr herpesvirus genomes by human APOBEC3 cytidine deaminases in culture and in vivo. J Virol **2011**; 85:7594–602.
33. Delebecque F, Suspene R, Calattini S, et al. Restriction of foamy viruses by APOBEC cytidine deaminases. J Virol **2006**; 80:605–14.
34. Mahieux R, Suspene R, Delebecque F, et al. Extensive editing of a small fraction of human T-cell leukemia virus type 1 genomes by four APOBEC3 cytidine deaminases. J Gen Virol **2005**; 86:2489–94.
35. Lemoine F, Gascuel O. Gotree/goalign: toolkit and go API to facilitate the development of phylogenetic workflows. NAR Genom Bioinform **2021**; 3:lqab075.

36. Minh BQ, Hahn MW, Lanfear R. New methods to calculate concordance factors for phylogenomic datasets. Mol Biol Evol **2020**; 37:2727–33.
37. Rambaut A, Lam TT, Max Carvalho L, Pybus OG. Exploring the temporal structure of heterochronous sequences using TempEst (formerly path-O-gen). Virus Evol **2016**; 2:vew007.
38. Stamatakis A. RAxML version 8: a tool for phylogenetic analysis and post-analysis of large phylogenies. Bioinformatics **2014**; 30:1312–3.
39. Anderson BD, Ikeda T, Moghadasi SA, Martin AS, Brown WL, Harris RS. Natural APOBEC3C variants can elicit differential HIV-1 restriction activity. Retrovirology **2018**; 15:78.
40. Jackson B. gofasta: command-line utilities for genomic epidemiology research. Bioinformatics **2022**; 38:4033–5.
41. Gigante CM, Korber B, Seabolt MH, et al. Multiple lineages of monkeypox virus detected in the United States, 2021-2022. Science **2022**; 378:560–5.
42. Dumonteil E, Herrera C, Sabino-Santos G. Monkeypox virus evolution before 2022 outbreak. Emerg Infect Dis **2023**; 29:451–3.
43. Luna N, Munoz M, Bonilla-Aldana DK, et al. Monkeypox virus (MPXV) genomics: a mutational and phylogenomic analyses of B.1 lineages. Travel Med Infect Dis **2023**; 52:102551.
44. Dang Y, Abudu A, Son S, et al. Identification of a single amino acid required for APOBEC3 antiretroviral cytidine deaminase activity. J Virol **2011**; 85:5691–5.
45. Johnston SC, Lin KL, Connor JH, Ruthel G, Goff A, Hensley LE. In vitro inhibition of monkeypox virus production and spread by interferon-beta. Virol J **2012**; 9:5.
46. Priyamvada L, Burgado J, Baker-Wagner M, et al. New methylene blue derivatives suggest novel anti-orthopoxviral strategies. Antiviral Res **2021**; 191:105086.
47. Wardle J, Burgers PM, Cann IK, et al. Uracil recognition by replicative DNA polymerases is limited to the archaea, not occurring with bacteria and eukarya. Nucleic Acids Res **2008**; 36:705–11.